Estimation of Acoustic Particle Motion and Source Bearing Using a Drifting Hydrophone Array Near a River Current Turbine to Assess Disturbances to Fish

Paul G. Murphy

A thesis

submitted in partial fulfillment of the

requirements for the degree of

Master of Science in Mechanical Engineering

University of Washington

2015

Committee:

Peter H. Dahl

Brian Polagye

David Dall'Osto

Program Authorized to Offer Degree:

Mechanical Engineering

University of Washington

Abstract

Estimation of Acoustic Particle Motion and Source Bearing Using a Drifting Hydrophone Array Near a River Current Turbine to Assess Disturbances to Fish

Paul G. Murphy

Co-Chair of the Supervisory Committee:
Professor Peter Dahl
Mechanical Engineering

Co-Chair of the Supervisory Committee:
Professor Brian Polagye
Mechanical Engineering

River hydrokinetic turbines may be an economical alternative to traditional energy sources for small communities on Alaskan rivers. However, there is concern that sound from these turbines could affect sockeye salmon (*Oncorhynchus nerka*), an important resource for small, subsistence based communities, commercial fisherman, and recreational anglers. The hearing sensitivity of sockeye salmon has not been quantified, but behavioral responses to sounds at frequencies less than a few hundred Hertz have been documented for Atlantic salmon (*Salmo salar*), and particle motion is thought to be the primary mode of stimulation. Methods of measuring acoustic particle motion are well-established, but have rarely been necessary in energetic areas, such as river and tidal current environments. In this study, the acoustic pressure in the vicinity of an operating river

current turbine is measured using a freely drifting hydrophone array. Analysis of turbine sound reveals tones that vary in frequency and magnitude with turbine rotation rate, and that may sockeye salmon may sense. In addition to pressure, the vertical components of particle acceleration and velocity are estimated by calculating the finite difference of the pressure signals from the hydrophone array. A method of determining source bearing using an array of hydrophones is explored. The benefits and challenges of deploying drifting hydrophone arrays for marine renewable energy converter monitoring are discussed.

TABLE OF CONTENTS

LIST OF FIGURES

ACKNOWLEDGEMENTS

This work was funded by the National Science Foundation through the Sustainability of Tidal Energy Grant and by the Department of Energy though the NNMREC Grant.

Chapter 1. INTRODUCTION

At present, many riverine villages in remote areas of Alaska receive most of their power from diesel generators. The lack of a road network requires fuel to be delivered by barge or air, resulting in high energy costs. Consequently, there is interest in developing turbines to harness the kinetic energy from the currents of nearby rivers, much in the same manner that wind turbines harness the kinetic energy in atmospheric winds.

An evaluation of the economic utility of river turbines to riverine communities should include an assessment of the effects of turbine presence and operation on fishes, particularly sockeye salmon (*Oncorhynchus nerka*), a vital resource for residents of subsistence based villages. The salmon population is similarly essential to the economic health of the commercial fishing and sport fishing industries. For these reasons, assessing risk to fish is a necessary step in evaluating the environmental and social compatibility of river turbines.

Sound is a pressure wave which generates minute motion in the fluid medium through which it propagates. Movement of the medium when disturbed by sound waves can be described in terms of discrete fluid particle motion, wherein fluid particles are defined as the smallest volume over which a calculation of density would still equal the average density of the fluid [1]. This acoustic particle motion is thought to be the primary mode of acoustic stimulation in many species of fishes, including sockeye salmon (*Oncorhynchus nerka*) [2]. Although it is unlikely that sound from turbines will be intense enough to cause physical harm to individual fish, behavioral changes that result in a decrease in the overall fish population (e.g., by discouraging the regular migration of salmon to spawning locations) are conceivable [3]. The effects of sound on fish behavior is an active area of research in the biological research community and this paper focuses primarily on quantification of turbine sound.

In this study, acoustic pressure is measured near a river current turbine, and properties of the turbine-generated sound are analyzed and discussed. Pressure

measurements are made using vertically separated and temporarily coherent hydrophones deployed from a drifting platform, from which the vertical components of acoustic particle velocity and acceleration are also estimated.

1.1 ACOUSTICS OF RIVER ENVIRONMENTS

The domain of a river, as it pertains to sound propagation, may be described quite generally as a depth varying channel with the average depth (D) usually small relative to the average width (W), and the average width small compared to the river length (L). For our frequencies of interest, of order 10-1000 Hz, a river can be considered a shallow water environment bounded by a pressure release surface above (air) and a sediment bottom characterized by higher density and sound speed than water. (An exception being very mud-like sediments found in slow moving rivers although such systems are of less relevance in energy conversion). Depth variation in a river occurs in both the across-channel and along-channel directions, which can have a strong effect on sound propagation. The term "along-channel" is used to describe a plane parallel to the bulk fluid motion, and "across-channel" to describe a plane perpendicular to the bulk fluid motion.

Sound emitted from a sound source in shallow water, at mid-water depth, will spread spherically until the wavefront reaches the top and bottom boundaries. Within this region, defined roughly by the water depth (H), the sound intensity will decrease in proportion to the inverse of r^2 (spherical spreading) where r is the range from the source. For ranges beyond H, roughly speaking, intensity falls with the inverse of r (cylindrical spreading), a result of reflection from the surface and bottom. In a river, the width (W) is generally greater than depth, but of a similar order; therefore, beyond the region of spherical spreading, an assumption of azimuthally symmetric (cylindrical) spreading is invalid.

Because a river environment is generally shallow relative to the acoustic wavelengths of interest (O 15 m for 100 Hz), sound propagation is best described in the context of normal modes. Normal mode solutions to the acoustic wave equation in shallow

water consist of a finite sum of trapped normal modes and an infinite (continuous) sum of untrapped modes [4]. The latter (or "leaky") modes leak energy into the bottom and thus experience a high loss during propagation, while the trapped modes can propagate over longer distances as the sound field is more effectively confined within the surface and bottom boundaries. An approximate rule for sound being trapped in the waveguide (i.e., for trapped modes to exist) is that the frequency satisfies $\frac{2H}{\lambda} > 1$, where λ is the wavelength of sound. Frequencies for which this ratio is < 1 are said to be below modal cutoff. In the along-channel direction, river depth may vary considerably over short distances. As a result, a sound field generated in deeper regions of the river and consisting of trapped modes may be subject to modal cutoff as the field propagates into shallower regions. In the across-channel direction, the river bottom generally slopes upward towards the shore on either side, resulting in modal cutoff at higher frequencies nearer to the shore.

Although modal cutoff and depth variation can limit the propagation of low frequency sounds, migratory fish may have no alternative but to travel through ensonified areas. Furthermore, since the width and depth of the channel in the vicinity of a sound source may be small relative to the wavelengths of sound produced by the source, it is important to quantify sound levels in the near field to fully assess the exposure of migrating fish.

Prior investigations have shown that the highest noise levels (measured in 1/3 octave bands) in rivers with no major obstructions to the flow and limited surface agitation (i.e., "runs") occur at low frequencies (< 50 Hz) [5]. Noise levels can be expected to decrease with a slope of approximately 30 dB/decade until around 250 Hz before increasing again with an average slope of approximately 6 dB/decade until 16 kHz. In addition to the general trends, a slight increase in level is expected from 500 Hz – 2 kHz.

1.2 River Turbine Sound Mechanisms

Data on sound from hydrokinetic (river, tidal, or ocean current) turbines is scarce, and there are no known measurements of particle motion near operating hydrokinetic turbines. However, one can draw on experience with analogous technology to anticipate possible sound sources. Much like wind turbines, periodic blade passage by stationary objects can create pressure minima and maxima during each revolution, which may generate propagating sound [6]. Sound generated in this way would be at frequencies directly related to the fundamental rotation rate of the turbine, with harmonics at higher frequencies. Broadband levels are also expected to vary with inflow velocity.

The generator used to convert mechanical to electrical power can also produce noise. The primary mechanism of sound generation from AC generators is vibration of the stator and foundation by periodically varying magnetic forces, which are caused by the generator's rotating magnetic field [7]. The number of magnetic pole pairs on the rotor or stator affects the forcing function, so sounds from generator vibration are related to both the rate of rotation and the particular number of pole pairs in a generator's design. Excitation of vibrational modes in the generator stator and foundation can significantly increase the amplitude of radiated sound. Gearboxes and vibration in the turbine foundation or rotation of shaft bearings may also produce sound.

While sound from turbulence generated by the rotation of the turbine or from vortices shed from the frame are also possible, the effectiveness of turbulent sources to radiate sound is weak owing to the quadrapole nature of such sources [8]. However, turbulent excitation of the blades can radiate sound more efficiently as a dipole source. The frequencies of this radiated sound would be expected to match the modes of blade vibration [9]. Finally, cavitation is well known to be a powerful radiator of sound as a monopole source, but hydrokinetic turbines are designed to avoid operating in a manner that promotes cavitation.

1.3 METRICS RELEVANT TO FISH HEARING RISK ASSESSMENT

Recent reports on fish hearing recommend the inclusion of particle motion measurements when assessing the risk that anthropogenic sound sources pose to fishes [3]. Behavioral audiograms, which show an animal's auditory threshold at a range of frequencies, have been developed for at least four species of fish, including Atlantic cod (*Gadus morhua*), Atlantic herring (*Clupea harengus*), Atlantic salmon (*Salmo salar*), and dab (*Limanda limanda*). While a high degree of caution has been advised in interpreting these data, they have provided some insight into fish hearing, and suggest the sensitivity of fish to lower frequency sounds of order 100-1000 Hz [3].

Although many fish species are sensitive to acoustic pressure, the majority exploit and are sensitive to the particle motion aspect of sound [2]. Located in the inner ear, the otolith has been identified as the principle organ responsible for sensation of particle motion and is thought to perform the function of an inertial sensor [2]. Fishes with a swim bladder or other gas filled sac may be capable of sensing sound pressure, provided the organ is located in close proximity to the ear. Salmon and trout, for example, do have a swim bladder, but it is not located close to the ear and therefore they are thought to be primarily sensitive to particle motion [3].

Although there is not an accepted standard for which quantity of particle motion should be reported, particle acceleration has been suggested as an appropriate metric given the current understanding of the otolith's function [2] [3].

1.4 SOURCE LOCALIZATION

Source localization by time delay of arrival estimation is a method of determining the angle of incidence of plane waves by examining the time that wavefronts arrive at adjacent hydrophones in an array. Source localization has been successfully used to track marine mammals, notably whales, by their vocalizations [10], and is of particular interest in marine energy converter monitoring studies because, unlike active acoustic methods, it

does not introduce a loud source into the marine environment. As loud sources may change the behavior of marine mammals, it is preferable to use passive methods of tracking when possible. In addition, real-time passive monitoring of marine energy sites (via communication cables) would consume significantly less bandwidth than active acoustic or video monitoring.

Chapter 2. METHODOLOGY

This section will describe in detail the basics of sound, the measurement theory utilized, the 'RivRaft' drifting platform and its instrumentation, the turbine site characteristics, and the specifics of deployment on the Kviachak River.

2.1 BASIC PROPERTIES OF WAVES AND SOUND

Waves are, in the most general sense, transitory disturbances caused by the movement of energy and information. When a wave interacts with a system, the state of the system is temporarily altered, but after the wave has passed, the system returns to its original state, although perhaps slightly altered by the wave's passing [1].

Waves are characterized by several principal properties. Frequency (f) describes the number of full oscillations of a wave as measured by a stationary observer over a period of time. The conventional unit of measurement of frequency is the Hertz (Hz), which has units of $1/s$. The inverse of frequency is known as the wave period (T), which is the number of seconds that elapse per oscillation. The wavelength (λ) of a wave is the distance from crest to crest of a wave.

Sound is a compressional wave that propagates through a material. The speed of sound, *c*, is set by the properties of the medium, and is related to frequency and wavelength by Eq. 2.1.1 [1], such that

$$\lambda f = c \,. \tag{2.1.1}$$

Typical sound speeds in air are approximately 343 m/s, while speeds in water are around 1500 m/s. The significant difference in speed is, primarily, a result of the higher density of water. Underwater sound speed also varies as a function of temperature, depth, and salinity. In the ocean, spatial variations in these parameters cause sound to propagate

in fascinating ways, making the *sound speed profile* an important property to characterize. Relationships between temperature, depth, and salinity typically take forms similar to [11]

$$c = 1449.2 + 4.6T - 0.055T^2 + 0.00029T^3 + (1.34 - 0.01T)(S - 35) + 0.016z \qquad 2.1.2$$

2.2 Source Bearing Estimation by Time-Delay of Arrival Estimation

A method to determine the bearing of an acoustic source relative to an array of hydrophones is described by Wahlberg [10]. For two or more hydrophones coherently measuring incoming sound, the time delay of arrival (TDOA) of each wave-front will differ with hydrophone position. Provided the distance from the source to the hydrophone pair is long relative to the spacing between hydrophones, L_{mn}, wave-fronts can be approximately as plane waves. This assumption, in combination with knowledge of the TDOA, denoted τ_d, allows calculation of the angle of incidence of the arriving plane wave (Eq. 2.2.1 and Figure 1), given by

$$\cos(\alpha_{mn}) = \frac{c\tau_d}{L_{mn}}. \qquad 2.2.1$$

In Eq. 2.2.1, c is the speed of sound and α_{mn} is the angle between an arriving plane wave and the axis of the receiver pair. A complex solution arises for values of $c\tau_d / L_{mn}$ exceeding a magnitude of 1. In practice, this can occur if the $r >> L$ assumption is not valid, implying non-planar wavefronts. Error in TDOA estimation, which may result from noise or receiver motion and orientation changes, can also result in complex results. Time

delay of arrival can be estimated by examining the cross-correlation $R_{ab}(\tau)$ between two signals $a(t)$ and $b(t)$, (Eq. 2.2.2)

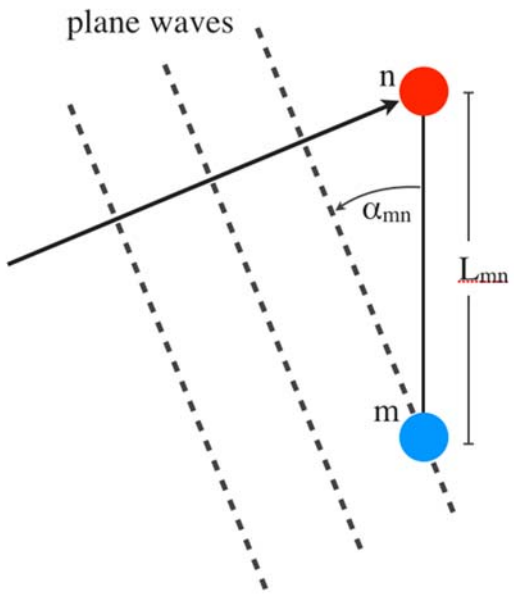

Figure 1: Source Localization Theory. Angle of incidence is calculated from the time delay of arrival of plane waves at spatially separated coherent hydrophones.

$$R_{ab}(\tau) = E\left[a(t)b(t+\tau)\right] \qquad 2.2.2$$

where E is the expected value function. The index of the maximum of the cross-correlation function provides an estimate of the time delay of arrival between two hydrophones. In this case, the hydrophone producing signal b is assumed to be further from the source. As seen in Figure 2, lag at the maximum cross correlation can take on small values for two closely spaced hydrophones,

Higher resolution in source localization measurements can be achieved by changing one of the three parameters on the right hand side of Eq. 2.2.1. Increasing L_{mn} generally results in a larger time delay of arrival at adjacent hydrophones. However, increasing L_{mn} increases the minimum range for which a wave can be assumed to be planar. Alternatively, increasing τ_d by means of using measuring at higher sample rates can easily increase resolution. Finally, using multiple hydrophone pairs can increase accuracy substantially.

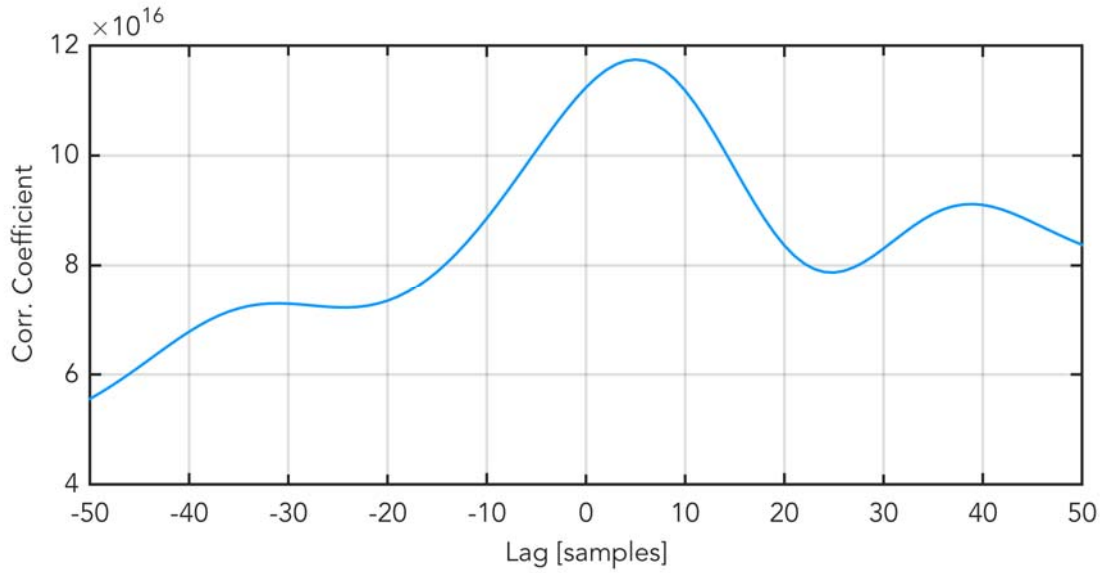

Figure 2: Example cross-correlation from closely spaced hydrophones.

Calculation of the bearing angles for a multiple receiver array goes as (Eq. 2.2.3) [10]

$$(r_x(i)-s_x)^2+(r_y(i)-s_y)^2+(r_z(i)-s_z)^2=c^2(T_1+t(i))^2 \qquad 2.2.3$$

where the coordinates $r_x(i)$, $r_y(i)$, and $r_z(i)$ correspond to the position of each receiver. The coordinates s_x, s_y, and s_z correspond to the position of the source. The bearing angles

relative to the Cartesian axes can be calculated by solving a system of equations based on Eq. 2.2.3 (Eqs. 2.2.4 through 2.2.8) [10],

$$(\vec{r}_i - \vec{r}_j\ )\cos\left(\theta_{ij}\right) = c\tau_{ij} \tag{2.2.4}$$

$$Ax = b \tag{2.2.5}$$

$$A^T Ax = A^T b \tag{2.2.6}$$

$$(A^T A)^{(-1)} A^T Ax = (A^T A)^{(-1)} A^T b \tag{2.2.7}$$

$$x = (A^T A)^{(-1)} A^t b \tag{2.2.8}$$

where x is a vector of cosines of the bearing angles. The bearing angles can be determined by taking the inverse cosine of x, such that

$$\alpha = \cos^{-1}(x_1) \tag{2.2.9}$$

$$\beta = \cos^{-1}(x_2) \tag{2.2.10}$$

$$\gamma = \cos^{-1}(x_3). \tag{2.2.11}$$

Finally, the azimuth and elevation angles can be calculated (Eqs. 2.2.12 and 2.2.13) as

$$\theta = \tan^{-1}\left(\frac{\beta}{\alpha}\right) \tag{2.2.12}$$

$$\varphi = \tan^{-1}\left(\frac{\left(\alpha^2 + \beta^2\right)^{\frac{1}{2}}}{\gamma}\right). \tag{2.2.13}$$

Where θ is the azimuth angle and ϕ is the elevation angle.

2.3 SITE CHARACTERISTICS

The Kviachak River flows from Lake Iliamna to Bristol Bay in southwest Alaska (Figure 3). The village of Igiugig sits at the headwaters of the Kviachak River and currently generates most of its electricity from diesel generators. Near the site river currents often exceed 2 m/s, turbidity is low, and the river is largely free of debris, making it a particularly good candidate for hydrokinetic power generation.

At the turbine deployment site, the river bed is predominantly small cobbles (less than 10 cm diameter), overlying gravel and coarse sand. Based on the shoreline composition, the cobble layer likely overlays fine, unconsolidated sediments. Closer to the river mouth, the bottom was composed of much finer sand and little cobble, while downstream of the turbine site the bottom composition varied between regions primarily composed of coarse sand and gravel and regions dominated by small cobbles. The average water temperature in the vicinity of the turbine was 16 °C, measured at a depth of 1 m on August 21 and 24, which, with zero salinity (freshwater), results in a sound speed of approximately 1469 m/s [11].

There are abundant fish in the Kviachak River, most notably sockeye salmon. Each year, these salmon migrate up the Kviachak to Lake Iliamna to spawn. Adult salmon typically swim upstream through the shallow edges of the Kviachak, where flow rates are lower to conserve energy for spawning, while juvenile salmon outmigrating to the ocean are found to swim through the generally faster and deeper channels near the middle of the river.

Figure 3: RivGen Site. The village of Igiuig on the Kviachak River, flowing from Lake Iliamna (left, out of frame). The turbine location and coordinate system are shown with satellite view of the village of Igiugig (left). Local bathymetry and locations of upstream anchors can be seen (right). Position of turbine is approximate.

2.4 River Turbine

A RivGen river current turbine, developed by the Ocean Renewable Power Company (ORPC), was installed on the Kviachak River in August 2014. The RivGen (Figure 4) turbine is a helical, cross-flow turbine (horizontal orientation) designed to produce power from river currents. The RivGen turbine has five principal components: turbine rotor, generator, support frame, pontoons, and power export cable to a shore station. During deployment, the turbine is towed to location and moored to upstream anchors. The generator is a 3-phase AC direct drive design (no gearbox), and, for initial characterization testing, rotation rate is varied by application of a resistive load at a shore station. When the applied resistive load results in a rotation rate that maximizes power output, the turbine is said to be operating optimally. At low resistance, the generator approaches a short-circuit operating condition and produces enough opposition torque to bring the turbine to a stop. In a commercial operation, the power delivered to shore would connect with the local electricity grid.

The RivGen turbine is submerged in an area with an average depth of 5 meters. Because of the height of the turbine foundation, the rotational-axis depth is approximately 2.5 meters.

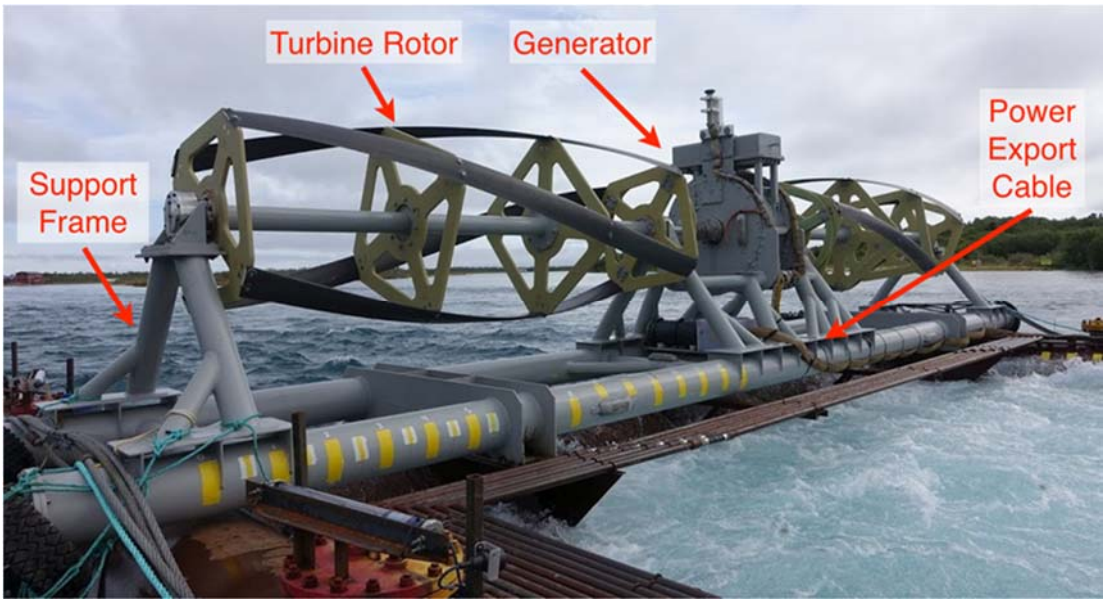

Figure 4: RivGen Turbine. The ORPC RivGen turbine moored and floating on the surface of the Kviachak River during maintenance.

2.5 'RivRaft' Drifting Hydrophone Array

As sound waves pass through a medium, fluid particles are disturbed in an oscillatory manner that is well described by the Navier-Stokes equations [1]. Because viscous effects are neglected, it is common to see the Euler equations referenced instead. It is convenient in underwater acoustics to linearize the Euler equations, thus reducing their complexity without a significant loss of accuracy. Estimation of particle motion follows from a substitution in the linearized Euler equations.

In this study, we estimate particle acceleration using a finite difference approximation for the pressure gradient from coherent and spatially separated hydrophones [12]. Beginning with the linearized Euler equation [13]

$$\nabla p(t) = -\rho_0 \vec{a}(t), \qquad 2.5.1$$

where $\nabla p(t)$ is the pressure gradient, $\vec{a}(t)$ is the particle acceleration, and is the density of the fluid, the approximation for particle acceleration given by the finite difference approximation becomes

$$a_{21}(t) = -\frac{\left(p_2(t) - p_1(t)\right)}{\rho_0 \, d}, \qquad 2.5.2$$

where $p_1(t)$ and $p_2(t)$ are the pressures at hydrophones 1 and 2, respectively, and *d* is the separation distance between hydrophones. To estimate particle acceleration for sound with wavelength λ with a maximum plane wave systematic intensity error of -0.5 dB, a hydrophone spacing of satisfying $d < \lambda/8$, is required [13]. An increase in bandwidth is afforded by decreasing *d*, however this results in higher phase errors at low frequencies, where the pressure field can take on smaller values at adjacent points. Therefore, it is advantageous to choose d such that only the highest frequencies (smallest wavelengths) of interest can be measured, as any additional reduction in *d* will result in increased error.

Particle velocity can be estimated by cumulatively integrating both sides of Eq. 2.5.2, such that

$$v_{21}(t) = -\int_{-\infty}^{t} \frac{\left(p_2(t) - p_1(t)\right)}{\rho_0 \, d} d\tau \, . \qquad 2.5.3$$

The physical environment of the acoustic near field of a hydrokinetic turbine complicates instrument deployment (currents on the order of a few meters per second). Freely drifting systems equipped to measure acoustic pressure around tidal turbines have been successfully deployed and are effective at minimizing contamination by “flow noise”,

which arises from differential velocity between hydrophone elements and water currents [14] [15]. The RivRaft (Figure 5) is a rigid and freely drifting platform that minimizes net fluid flow over the face of mounted hydrophones, thereby greatly reducing flow noise.

2.5.1 *Platform Design*

Because of the remoteness of the study site, the RivRaft was designed to ship disassembled be assembled on site, and be deployed/recovered by a small crew with minimal mechanical assistance. The RivRaft frame was constructed of 80/20 15-series ultra-lite extruded aluminum (Figure 5). The 80/20 frame permitted reconfiguration when necessary and was both lightweight and stiff. Buoyancy was provided by four 91 cm x 15 cm outer diameter pontoons (foam-core schedule 40 PVC). The overall weight of the instrumented system in air was

Figure 5: The RivRaft during deployment on the Kviachak, chandelier submerged (left). The chandelier with hydrophones and Doppler velocimeter in lowered position (right).

approximately 72 kg, and its reserve buoyancy was approximately 20 kg. The measurement array was at the base of a "chandelier" (Figure 6), a retractable, vertically oriented aluminum spar, which could be raised fully above the water line or lowered to a depth of up to 1.6 m. It was desirable for hydrophones to be positioned at moderate depth in the water to avoid close proximity with the water-air interface where the sound field vanishes. The chandelier supported up to four hydrophones (icListen HF, Ocean Sonics) in a tetrahedral arrangement, and the probe for an acoustic Doppler velocimeter (Nortek Vector). The spacing between hydrophones was originally set at 0.6 m, allowing estimation of particle velocity and acceleration up to 400 Hz, and was chosen based on the approximate hearing range of salmon. Following damage incurred to three hydrophones on August 18, a two-hydrophone vertical array was fabricated on site. In order to ensure that both hydrophones were as deep in the water as possible, a separation distance of 15.24 cm was used, allowing estimation of vertical particle velocity and acceleration up to 1200 Hz. Four lines (not pictured) tensioned the submerged chandelier to the surface frame to reduce vibrations. Hydrophones were shielded with cylindrical plastic guards made of perforated PVC. An in-water calibration (conducted in October, following deployment) revealed that overall voltage sensitivity and directional response of the hydrophones were not affected by shielding of this type at frequencies less than 6 kHz.

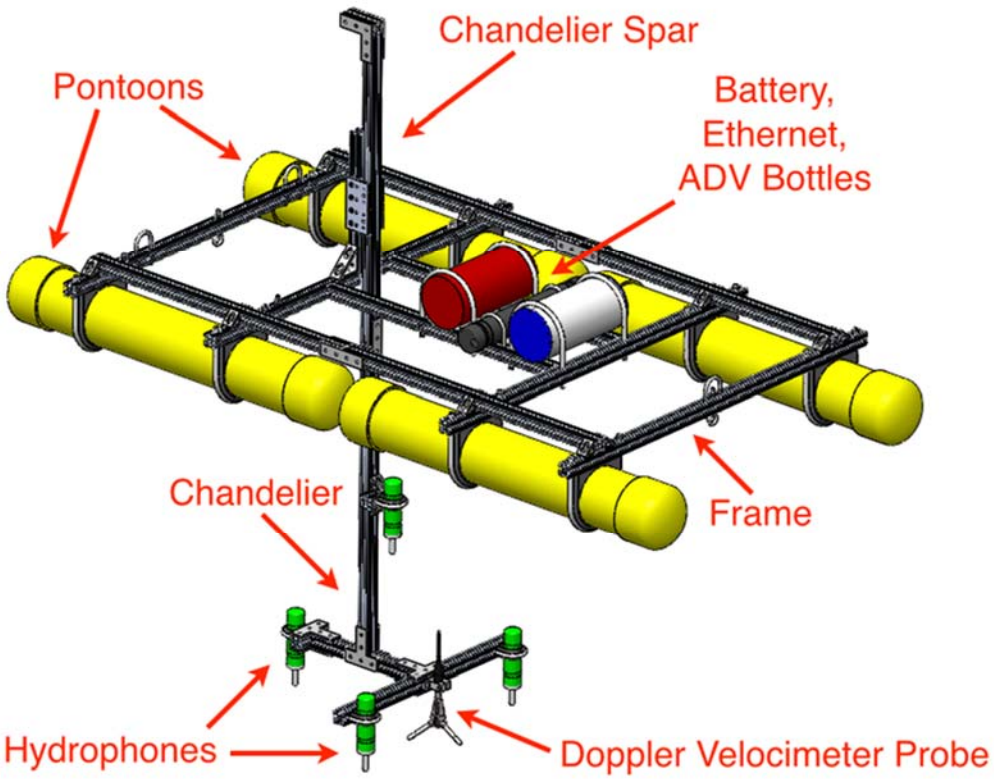

Figure 6: The RivRaft Design: Instrument cables, tensioning lines, and hydrophone flow shields not shown.

2.5.2 *Instrumentation*

The icListen HF hydrophones have a measurement bandwidth of 10 Hz – 200 kHz, a nominal sensitivity of -168 V/µPa, onboard A/D converter, internal storage, and onboard power. Prior to and following deployment, each hydrophone was calibrated using a M351 field calibrator (GeoSpectrum), which can produce traceable calibration tones at 10, 26, 70, 100, and 250 Hz. A pressure vessel containing an Ethernet switch was used to synchronize hydrophone signals in a master-slave configuration. The Ethernet switch and hydrophones were powered by an external battery pack in a second pressure housing. The Nortek Vector included an integrated inertial motion unit (IMU), allowing measurement of

relative motion between the raft and river and changes to orientation. The ADV probe was attached to the bottom of the chandelier to measure relative velocity as close to the array centroid as possible and, therefore, identify the potential for flow noise contamination. A GPS position logger (QStarz BT-Q1000eX) sampling at 1 Hz resolution was used to record raft position. Finally, two cameras (GoPro Hero 3) were included for video documentation. The first was fixed on the top of the chandelier post facing the bow, and the second submerged and fixed at the bottom of the chandelier post, facing the bow but angled downwards for a view of the river sediment.

2.6 Field Measurements

Acoustic experiments were conducted from August 14 through August 25, 2014. Sound from nearby fishing boats and rain were the primary sources of anthropogenic noise in the measurements and care was taken to document the occurrence of both.

A typical drift configuration is presented in Figure 7, showing the approximate scale of the turbine and nominal distance between the raft and turbine. The turbine location on the river was marked by several surface floats, such that the raft was consistently deployed at a lateral offset to limit the risk of entanglement. Several initial drifts were conducted on August 16 to determine best practices for working on the river. A location to the lee of a small island upstream of the turbine was identified as a suitable deployment site: sheltered from the high velocities in the river, close enough to shore to load and unload the raft from the skiff, and deep enough to lower the hydrophone chandelier while close to shore. From here, the raft was guided into faster currents using a boat hook and allowed to drift. After travelling at least 100 meters past the turbine, the raft was recovered by the skiff crew, the chandelier was retracted, and the raft was then towed to an area of slow flow downstream. At this location, the raft was loaded on to the skiff and returned to the upstream location for subsequent drifts.

Sound pressure and particle motion were measured with the turbine in one of two operational states: “braked” and “optimal”. When operating in “braked” mode, the turbine

was not rotating or generating power. When operating in "optimal" mode, a turbine rotated at a rate of approximately 50 rpm, which coincided with the optimal tip speed ratio [16].

During the preliminary drifts on August 16, three hydrophones were submerged with the lowest hydrophone 0.76 m below surface, but the raft was not equipped with a GPS tracker, ADV, or IMU. Following reconfiguration after hydrophone damage on August 18, measurements resumed on the 22, 24, and 25 with the reconfigured vertical orientation 2-hydrophone array. The analysis presented here focuses on data from August 25, on which total of five drifts were conducted. On August 25, hydrophone 1 was deployed at a depth of 0.61 m, and hydrophone 2 at a depth of 0.47 m (for a mean array depth of 0.53 m). For simplicity, the three braked cases will be referred to as Braked 1-3, and the two optimal cases as Optimal 1-2.

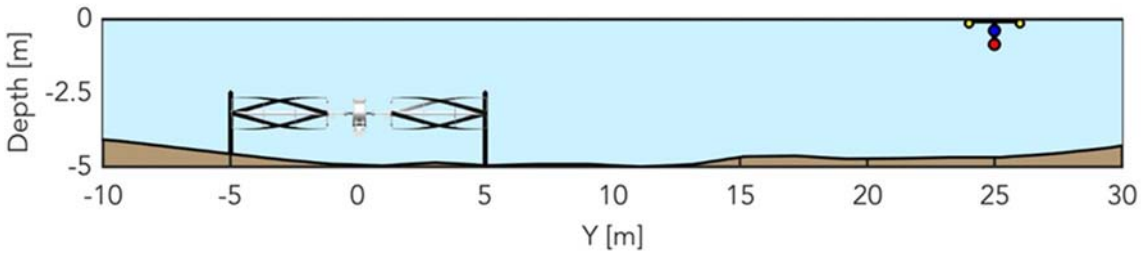

Figure 7: Cross-section of typical drift configuration. Raft shown with two element vertical array: hydrophone 1 (red), hydrophone 2 (blue).

2.7 DATA PROCESSING

2.7.1 *Sound Pressure Level and Pressure Spectral Density*

Sound pressure level and pressure spectral density are standard measures of sound are merit description. The sound pressure level (SPL),

$$SPL = 10log_{10}\left(\frac{p_{rms}^2}{p_0^2}\right) \qquad 2.6.1$$

is a ratio of the square of root mean square pressure, p_{rms}, to the square of a standard pressure, p_0, expressed logarithmically in units of decibels (dB) (Eq. 2.6.1). Because of the large dynamic range in acoustic measurements, logarithmic measures of magnitudes are particularly convenient. The pressure spectral density, given by

$$S_p(f) = \frac{2\left|\mathrm{F}\ \{x(t)\}\right|^2}{Nf_s} \qquad 2.6.2$$

is a measure of the distribution of variance in a pressure time series over frequency. Practically, pressure spectral density can be calculated only up to a maximum frequency, called the Nyquist frequency, which is equivalent to half of the sampling frequency used to measure the pressure time series. The pressure spectral density, $S_p(f)$, can be calculated by Eq. 2.6.2, where $\mathrm{F}\ \{x(t)\}$ is the Fourier transform of the pressure time series, N is the number of samples, and f_s is the sampling frequency.

The spectrum is calculated over discrete windows, or regularly sized segments, of the pressure series. Windows are averaged to produce the final spectrum. Because the FFT algorithm assumes periodic signals (a measured pressure time series is unlikely to be perfectly periodic), tapered windows help to reduce spectral leakage. A taper, such as a cosine taper, creates an artificially periodic signal. Windows are overlapped to compensate for the loss of information at the edges of each tapered window. Computationally, this requires the calculation of a higher number of FFTs, but overlaps of 50% are usually enough to provide an accurate measure of spectral distribution. Spectrograms are a way of viewing the change in pressure spectral density over time and are constructed by calculating the pressure spectral density in regular windows.

2.7.2 *Hydrophone Array*

The recorded voltage data are band-pass filtered in the time domain using a phase preserving method to exclude frequencies below 30 Hz and above 1200 Hz (where particle

motion measurements are not accurate), except for general considerations of broadband sound production by the turbine, for which the high pass filter is extended to 10 kHz. Recorded voltage data were sampled at 256 kHz, but subsequently down-sampled (after filtering) by a factor of 10 to reduce file size. The effective hydrophone sample rate after down-sampling is 25.6 kHz.

The recorded voltage time series are converted to pressure by first calculating the fast Fourier transform of the data, then multiplying by frequency dependent calibration curves obtained from the M351 field calibrator. After converting from complex voltage spectra to complex pressure spectra, an inverse Fourier transform is used to return to the time domain for further processing (such as time-domain calculation of particle motion). Frequency-dependent sensitivity curves are approximated by a cubic spline interpolation between discrete calibration frequencies (10, 26, 70, 100, 250 Hz). In general, hydrophone sensitivity varied between instruments at the same frequency by no more than 1 dB re 1 V/μPa and was flat above 250 Hz for individual instruments.

Time-domain pressure measurements and particle motion estimates are demeaned where appropriate and prior to subsequent spectral processing. Pressure spectral densities and spectrograms are calculated from the average of the pressure signals from hydrophones 1 and 2, such that pressure and motion spectra are presented for the same depth (~0.53 m).

Pressure spectrograms for analyzing low frequency sounds are produced using quarter second window (6400 samples) with cosine tapers (hamming) and 50% overlap. On occasion, transient "clicking" sounds were heard, and for these short duration signals pressure spectrograms are created using $1/16^{th}$ second windows (1600 samples) with a cosine taper (hamming) and 50% overlap. Pressure and particle acceleration spectral densities are calculated using MATLAB's "pwelch" function using quarter second windows (6400 samples) with cosine tapers (hamming) and 50% overlap, and are presented with 95% confidence intervals generated by the pwelch function.

As will be shown (Results, Acoustic Particle Motion), distinct spectral peaks are apparent in the "optimal" spectra and denoted H1, H2, and H3. The frequency of the H1 tone, which oscillates during a drift, is calculated by identifying the frequency with the

maximum spectral level in the 90-110 Hz band. Here, pressure spectral densities are calculated for 1.5 s long intervals. Each interval is assigned a location in the along-stream direction (x) corresponding to the raft position at the temporal mid-point of the interval. Each interval is demeaned and windowed into intervals with 6400 points with a cosine taper (hamming) and 50% overlap. RMS pressure for each tone is determined by integrating the spectra over a 5 Hz band centered at the peak frequency, and then calculating the square root of the result.

A result presenting the decay of the 1/3 octave band centered on 100 Hz with range for the Optimal 1 drift will be shown (Results). Calculations of 1/3 octave band levels are done in the frequency domain by integrating over calculated pressure spectral densities within the lower and upper limits of each band. Here, PSDs are calculated using half second windows over segments of 1.5 seconds. Range from the turbine is determined using the approximate raft position at the midpoint of each time segment. Maximum and minimum values of the braked data within a region without boat noise provide a measure of the ambient conditions on the river in the same band.

2.7.3 *ADV*

Relative velocity was measured in three directions, and the norm is calculated. The relative velocity between the raft and the current can be used to determine the spectral contamination from flow noise.

2.7.4 *GPS*

GPS data was recorded in degrees latitude and longitude, and is converted to Cartesian coordinates with the origin located at the turbine centroid (59.3247°N and -155.9151°W). The Cartesian coordinate system is rotated 107 degrees clockwise such that the turbine's rotational axis is oriented along the y-axis, and the river currents are approximately along the x-axis. Cubic interpolation from GPS data (sampled at 1 Hz) is used to approximate the raft position at any time, though GPS measurements are likely accurate to 5 meters at best.

2.7.5 *Correlation with Turbine Performance*

The turbine rotation rate (sampled at 1 Hz) was provided by Ocean Renewable Power Company. As with GPS data, cubic interpolation was used to approximate the velocity between sampled points to correlate turbine rotation rate with acoustic measurements. We note that this process involves three, asynchronous clocks: the clock on the master hydrophone (synchronized before deployment to the clock on a PC synchronized using Network Time Protocol), the clock on the Ocean Renewable Power Company data acquisition system (synchronized daily using Network Time Protocol), and the GPS logger (GPS time information). Consequently, the difference between clocks is likely to be much less than the 1 second time basis for which GPS and rotation rate information is available.

Chapter 3. RESULTS

3.1 RIVRAFT PERFORMANCE

The RivRaft's heading, pitch, and roll time series are indicative of the platform's stability (Figure 8). Similarly, the relative velocity between the river current and raft is indicative of the probable contamination by flow noise.

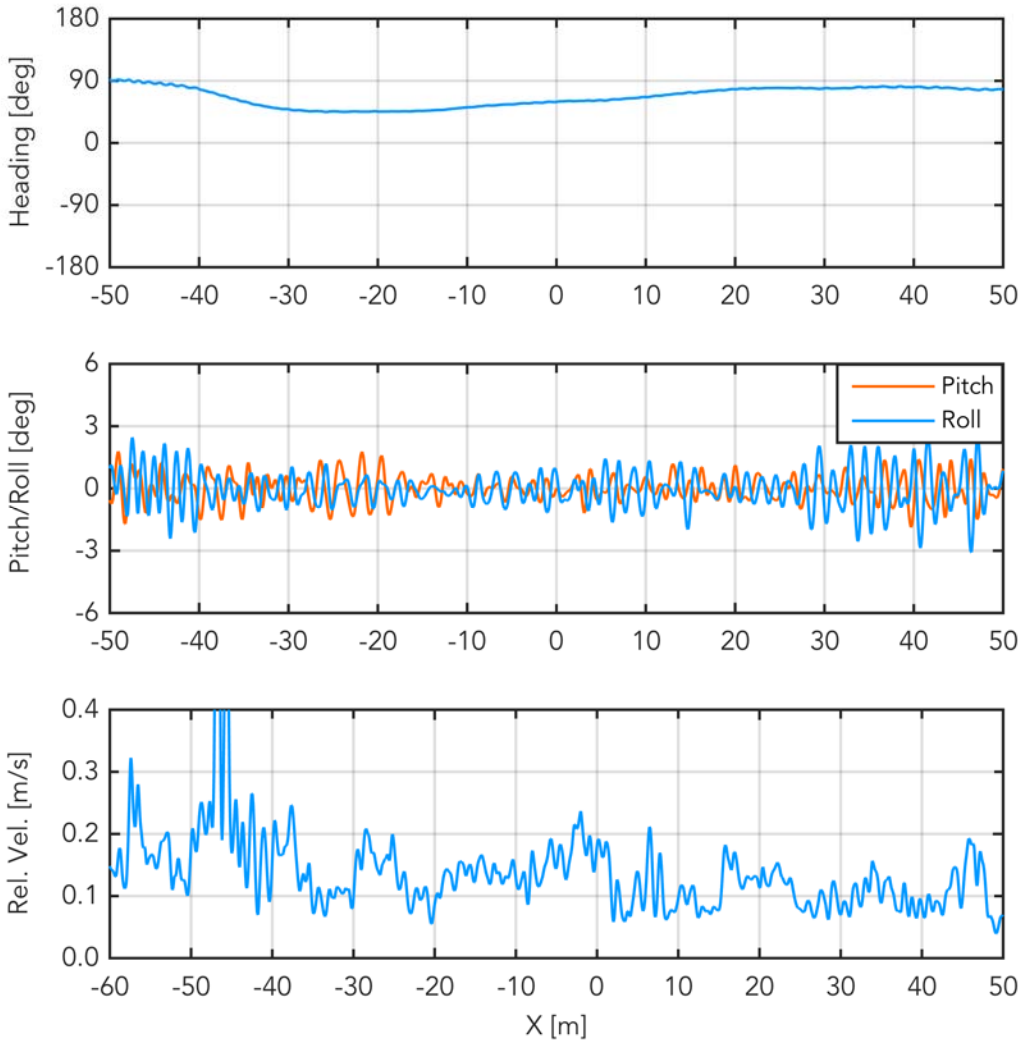

Figure 8: RivRaft Stability. Characteristic heading, pitch, roll, and relative velocity.

For relative velocities less than 0.5 m/s, flow noise is not expected to mask propagating sound at frequencies higher than order 10 Hz [14]. Because relative velocities were typically less than 0.3 m/s for RivRaft drafts, flow noise contamination is likely to be minimal.

3.2 Drift Paths

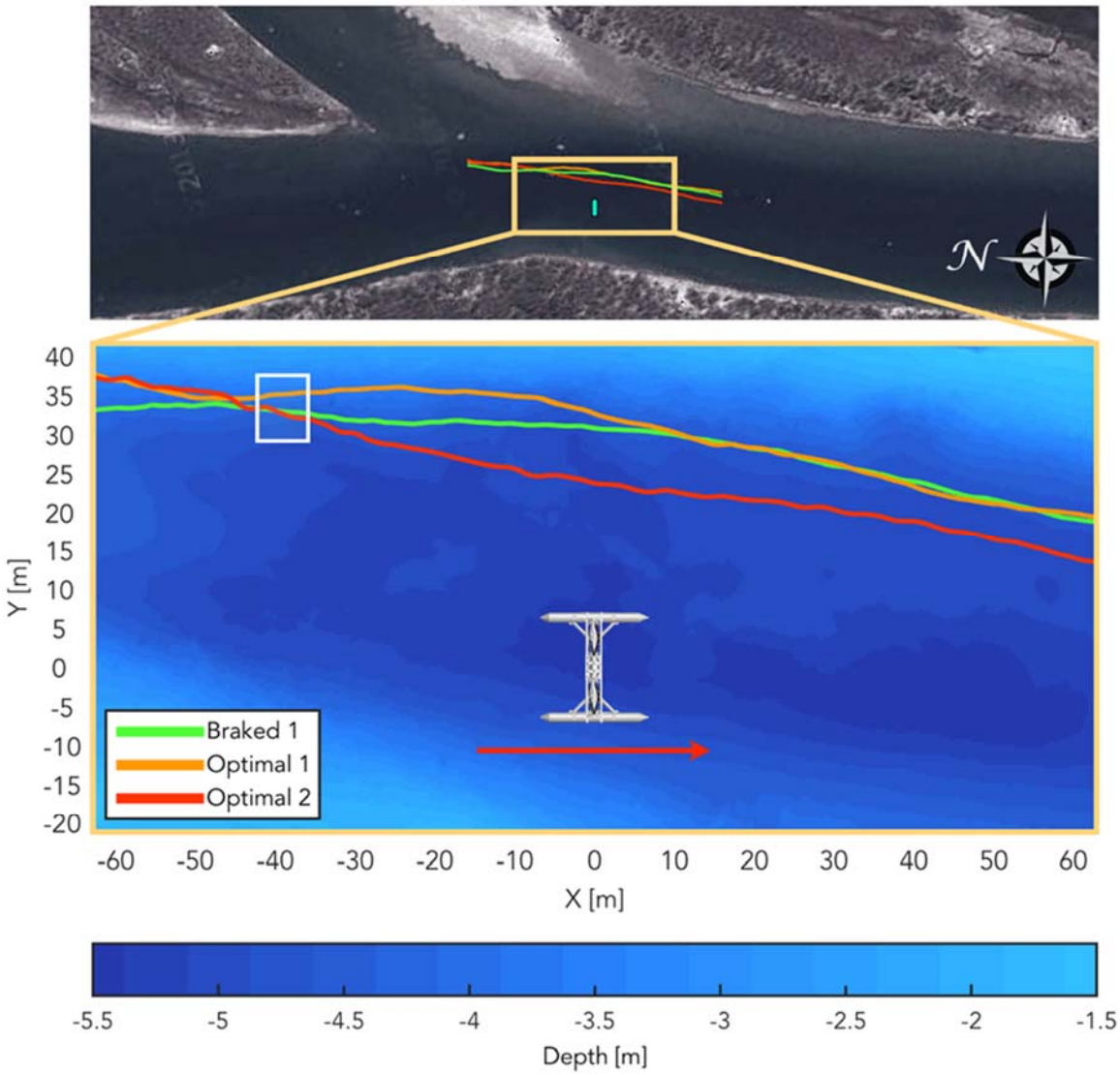

Figure 9: Bathymetry and Drift Paths. The bathymetry of the measurement area is shown with drift paths and turbine overlaid. The red arrow indicates flow direction. The white box denotes the region presented in Figure 13 and Figure 14.

The path taken by the RivRaft varied from drift to drift for the five cases considered (two "optimal", three "braked"). While two of the braked drifts are severely contaminated by significant boat noise from fishing vessels and not discussed here, the remaining braked

drift and both optimal drifts are relatively uncontaminated. These are overlaid on a plot of site bathymetry (Figure 9). The red arrow indicates the flow direction. The depths along the drift trajectories are typically 1-2 meters (20-40%) shallower than at the turbine deployment site (5 m depth).

3.3 ACOUSTIC PRESSURE

A spectrogram of the averaged pressure between both hydrophones from Optimal 1 (orange drift in Figure 10) reveals a tone centered at 100 Hz (Fig. 8).

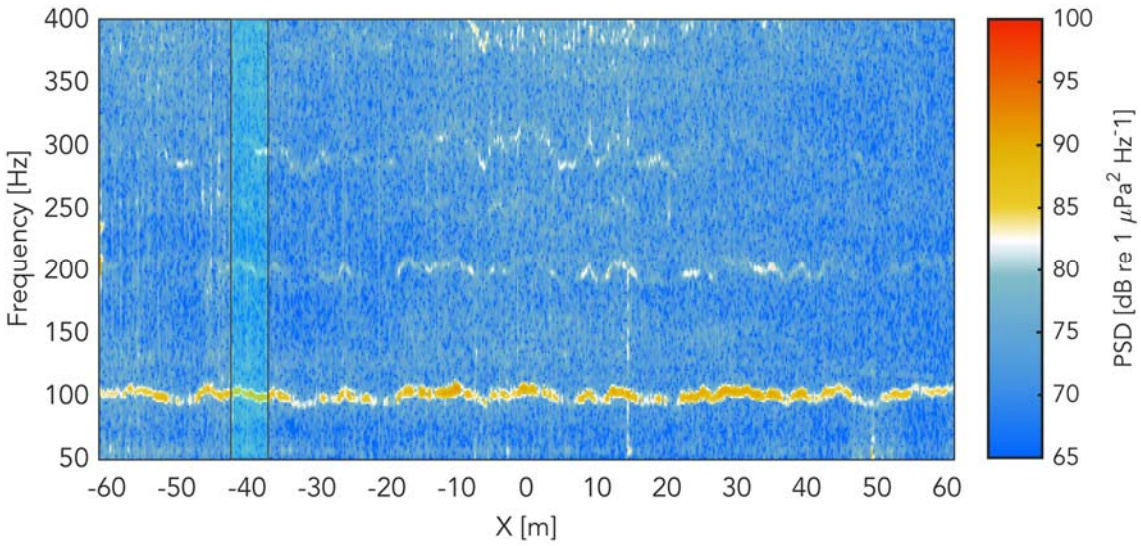

Figure 10: Pressure Spectrogram, Braked 1. A spectrogram of pressure from Braked 1 is shown. Boat noise contaminates the region of measurement from -20 m downstream of the turbine to approximately 50 m upstream of the turbine. The blue highlighted region denotes the area of analysis that corresponds to Figure 13 and Figure 14.

The center frequency of the 100 Hz tone appears to vary either in time or with distance from the turbine (a distinction that is not immediately clear because of the motion of the RivRaft during measurements). Tones at 200, 250, and 300 Hz with similar fluctuations in frequency are also visible, and tones centered at frequencies near 400 and 500 Hz may also be present, but are more difficult to distinguish from ambient noise.

Measurements while the turbine was braked contain boat noise from sport fishing traffic during portions of all drifts, which rendered braked drifts 2 and 3 unusable. A long period without boat noise from Braked 1 reveals that the 100 Hz and higher tones are not present while braked (Figure 11). It is notable that boat noise (occurring while the raft was between x = -20 m and x = 50 m, relative to the turbine), is similar in frequency and level to turbine sound for the 100 Hz harmonic, but without knowledge of the boat's position as a function of time, a direct comparison between sound produced by the turbine and fishing vessels is not possible.

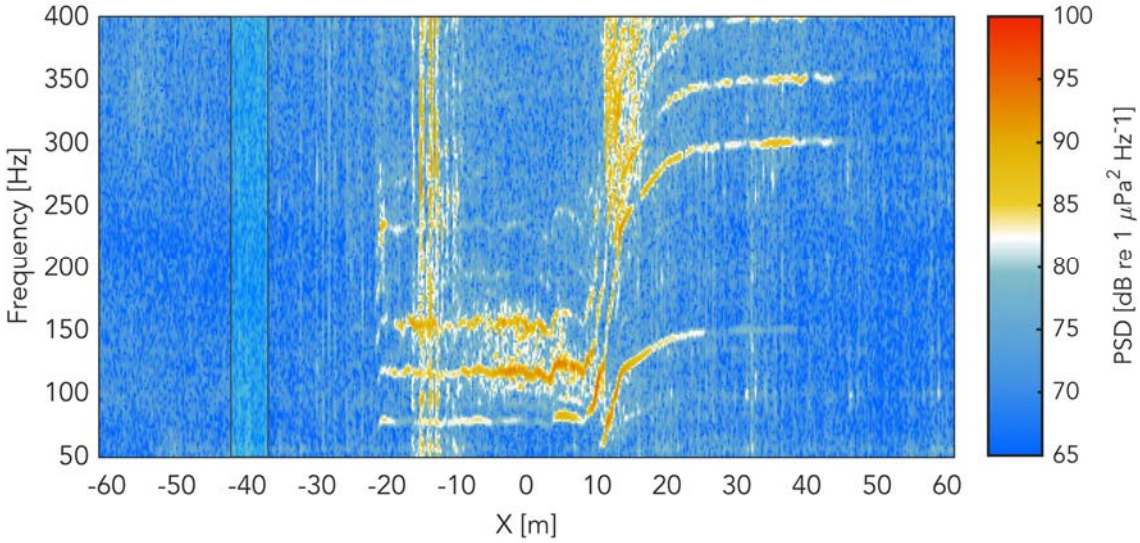

Figure 11: Pressure Spectrogram, Braked 1. A spectrogram of pressure from Braked 1 is shown. Boat noise contaminates the region of measurement from -20 m downstream of the turbine to approximately 50 meters upstream of the turbine. The blue highlighted region denotes the area of analysis that corresponds to Figure 13 and Figure 14.

In addition to the low frequency tones, a periodically occurring short duration broadband sound can be seen in the spectra at higher frequencies (Figure 12). This sound is audible in recordings and may be described qualitatively as a "clicking" sound. The "click" appears only when the turbine is operating.

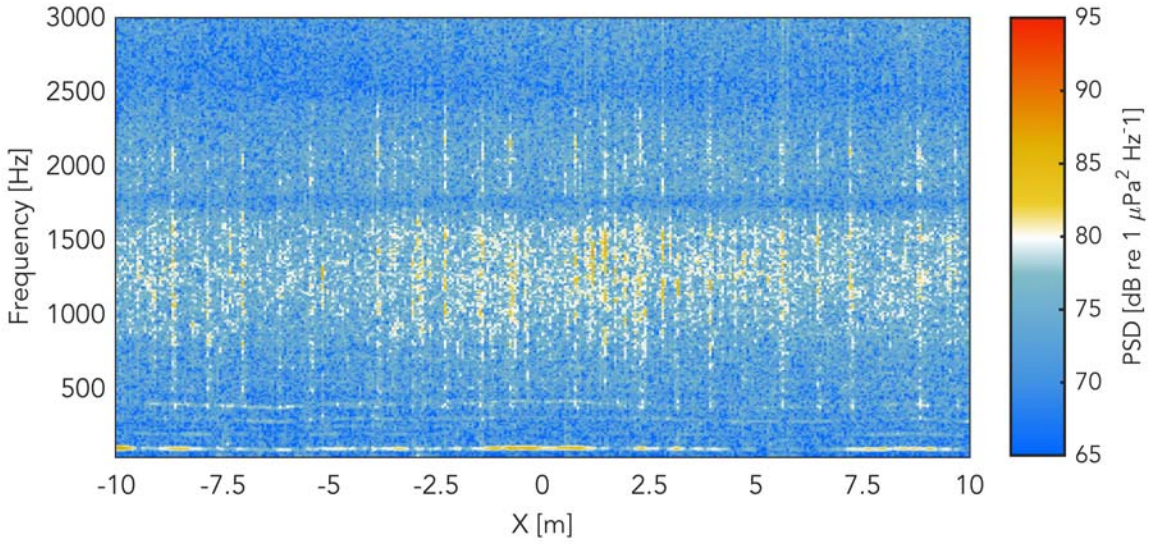

Figure 12: Clicking Noise. The broadband "clicking" noise is most visible in the 1000-2000 Hz band. Low frequency tones discussed previously are visible below 500 Hz.

A comparison of average pressure spectral density from Optimal 1 and Braked 1 over the region from x = -42 m to x = -38 m upstream of the turbine shows that the peak received level for the 100 Hz tone from the Optimal case can exceed the braked level (as close to a measure of background noise as is possible for this study) by as much as 30 dB re 1 µPa2 Hz-1 (Figure 13). Peak received levels for the 200 and 300 Hz tones can exceed braked levels by as much as 10 dB re 1 µPa2 Hz-1. In general, received levels above 100 Hz are higher for the optimally operating turbine than braked turbine.

The 100, 200, and 300 Hz tones are the most noticeable features of the optimal case spectra, and are present only during turbine operation. Because of their regular spacing and similar frequency fluctuations, it is plausible that they are harmonics. For clarity throughout the following sections, the tones appearing near 100, 200, and 300 Hz are denoted H1, H2, and H3, respectively.

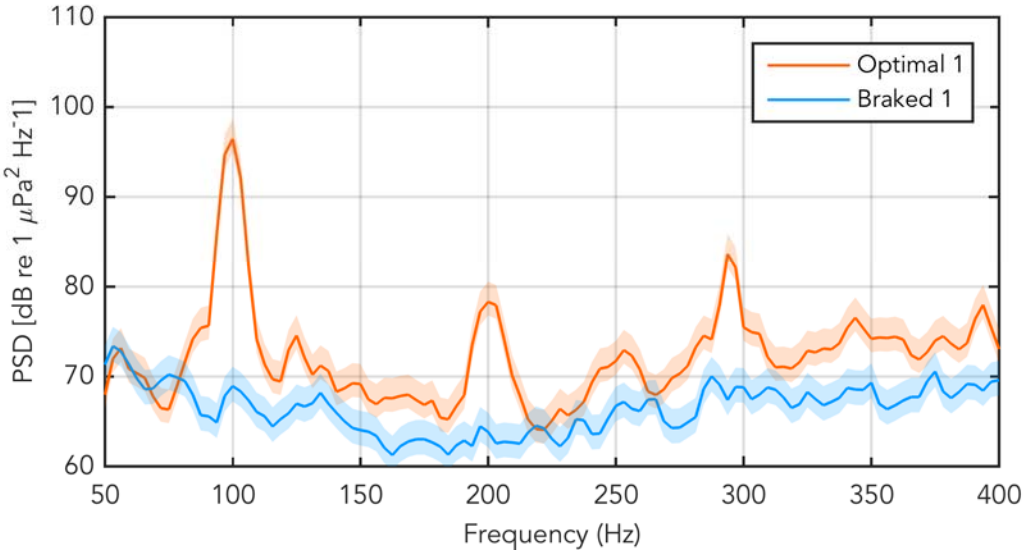

Figure 13: Pressure Spectral Densities of Braked 1 and Optimal 1. PSD for Braked 1 and Optimal 1 over the period when the raft was between x = -42 m to x = -38 m. The shaded regions show the boundaries of 95% confidence intervals.

3.4 Acoustic Particle Velocity and Acceleration

The tones in the pressure spectra are not clearly distinguishable in the vertical acceleration spectra (Figure 14).

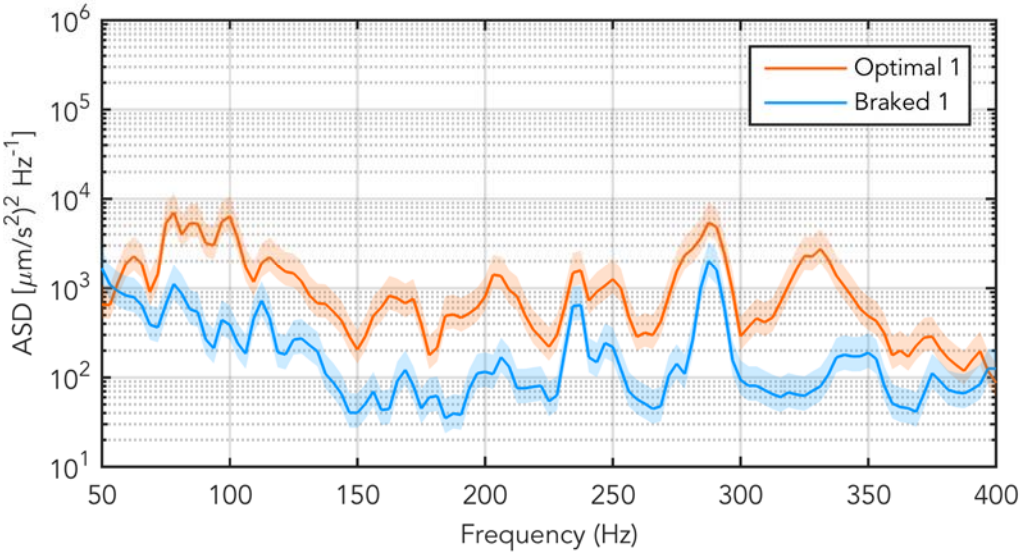

Figure 14: Acceleration spectral densities of Braked 1 and Optimal 1. ASD for Braked 1 and Optimal 1 over the period when raft was between x = -42 m to x = -38 m. The orange shaded region shows the boundaries of a 95% confidence interval.

The measured pressure spectral density can be compared to a prediction of the particle velocity by assuming that the measured sound propagates as a plane wave at all frequencies (Figure 15). Here, the left y-axis shows the measured pressure spectral density (Optimal 1, x = -40 m), and the right y-axis shows the predicted particle velocity spectral density based on the measured pressure. The measured particle velocity spectra density is plotted, which shows that the plane wave assumption is not valid at lower frequencies (at least less than 500 Hz).

An analysis of the river in the context of normal modes may explain this lack of agreement. Generally, the pressure field rolls off with decreasing distance from the air-water interface, while the particle velocity and acceleration take on their greater magnitudes. This effect is evident at greater depths from the air-water interface for lower frequencies, but is less significant for higher frequencies. Therefore, it is plausible that the vertical components of particle velocity and acceleration at 100 Hz are masked by other particle motion in the river at this depth (0.53 m).

Predicted particle velocity is near in value to the measured vertical particle velocity at frequencies above 500 Hz, indicating that the plane wave assumption is more accurate. Interestingly, between 750 and 1250 Hz, vertical particle velocity is less than the expected plane wave value, which may indicate that the horizontal component is more significant, while the vertical and component is approximately equal to the predicted particle velocity above 1250 Hz, indicating that most of the sound may be propagating vertically at these frequencies.

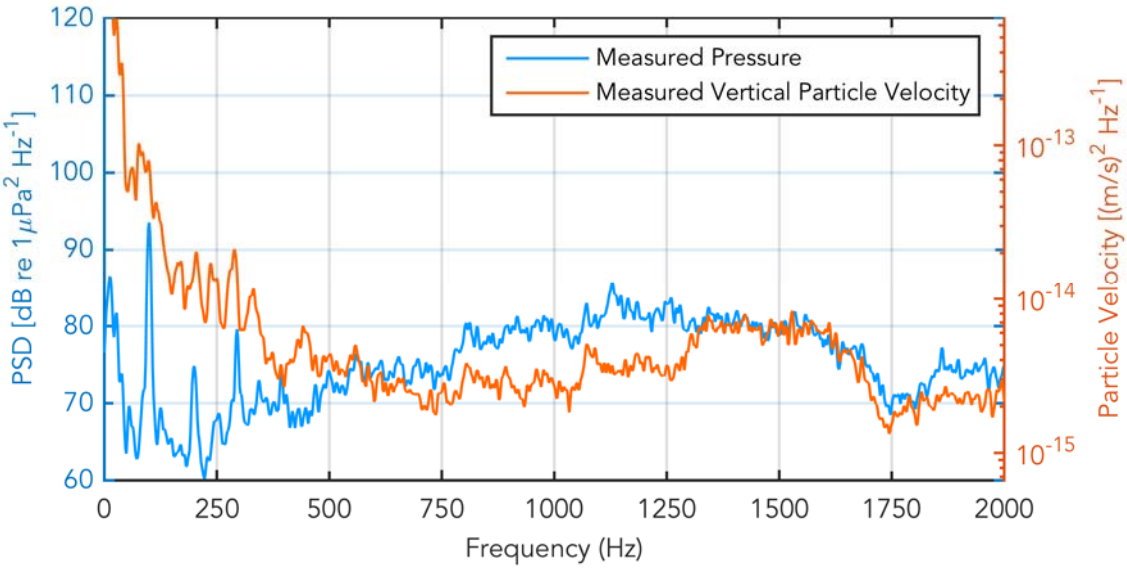

Figure 15: Measured pressure and particle velocity for Optimal 1 over the period when the raft was between x = -42m and x = -38 m. Using right axis, pressure may be interpreted as the predicted value of particle velocity following a plane wave assumption.

3.5 Magnitude and Frequency Variation in the H1 Tone

A comparison of the time series of the RMS pressure of the H1 (Optimal 1) tone to the angular velocity of the RivGen turbine shows these quantities are correlated in time (Figure 16). Similarly, the center frequency of the H1 tone also exhibits a strong correlation with turbine rotation rate. The variations in rotation rate are likely the effect of riverine

turbulence applied against a constant generator resistance (time-varying generator voltage and current) [17].

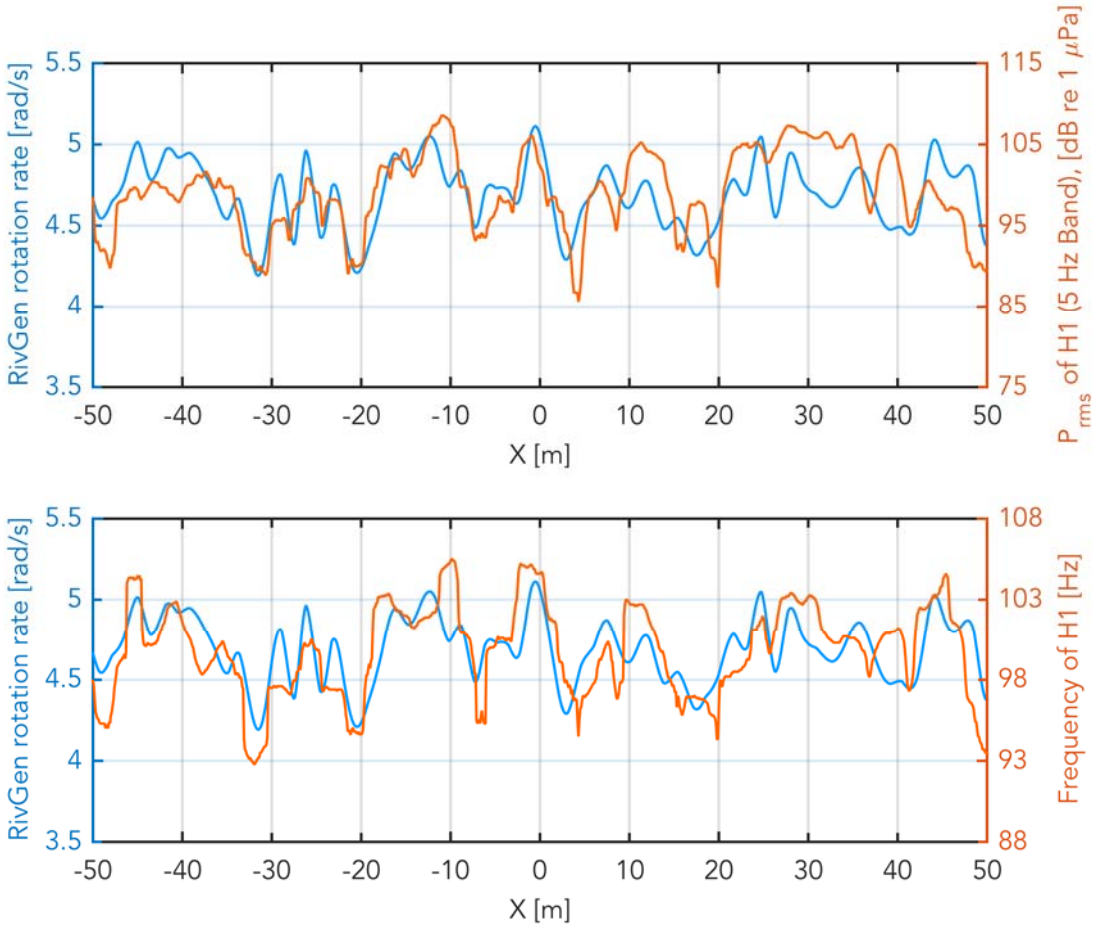

Figure 16: Turbine Rotation Rate, P_{rms} (integrated over 5 Hz band) and Frequency of H1 Tone (Optimal 1).

3.6 1/3 Octave Band Level Containing H1 Tone With Range

An analysis of the level of the 1/3 octave band centered on 100 Hz reveals that the 100 Hz tone for Optimal Drift 1 decays to within ambient levels within 125 m downstream

of the turbine (Figure 17). Here, the shaded blue region is bounded on top and bottom by the maximum and minimum values of the braked data in the same band.

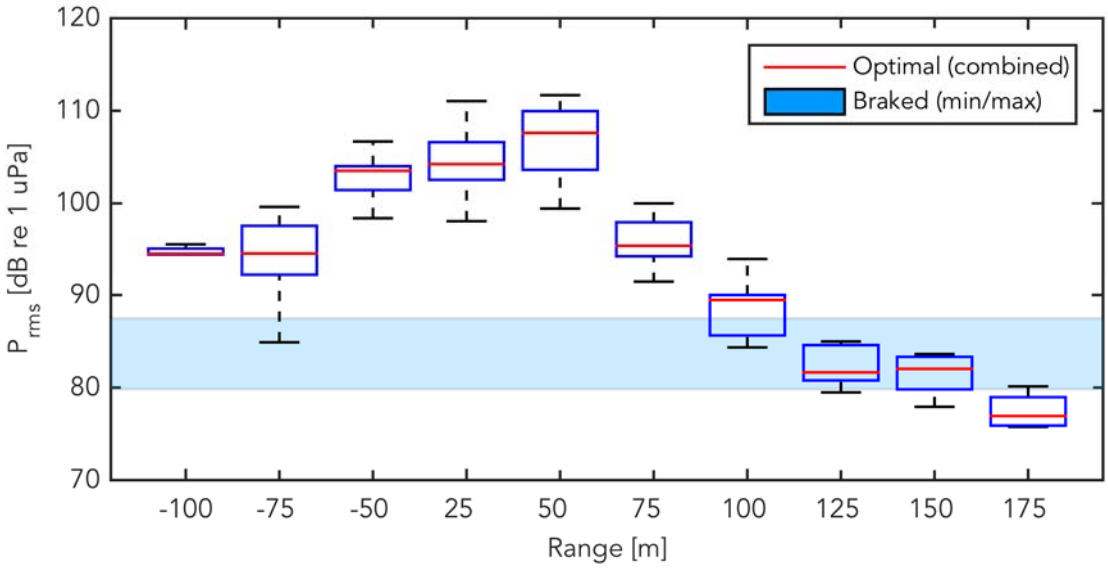

Figure 17: 1/3 Octave Band Level (centered at 100 Hz) of Optimal 1 with range. Negative ranges correspond to upstream positions, positive to downstream. The maximum and minimum values in the same band as measured when the turbine was braked provide a measure of the background levels.

3.7 Source Localization

The RivRaft was deployed from the R.V. Robertson for testing in Admiralty Inlet, Puget Sound, Washington on June 18th, 2014. At the time, the raft was equipped with a four hydrophone array with 0.6 m spacing between hydrophone elements and an array centroid depth of 1.3 m. During tests of the source localization methods, the raft was allowed to drift freely during a period of slack tide, and the R.V. Robertson remained with 30 meters of the raft at all times Figure 18.

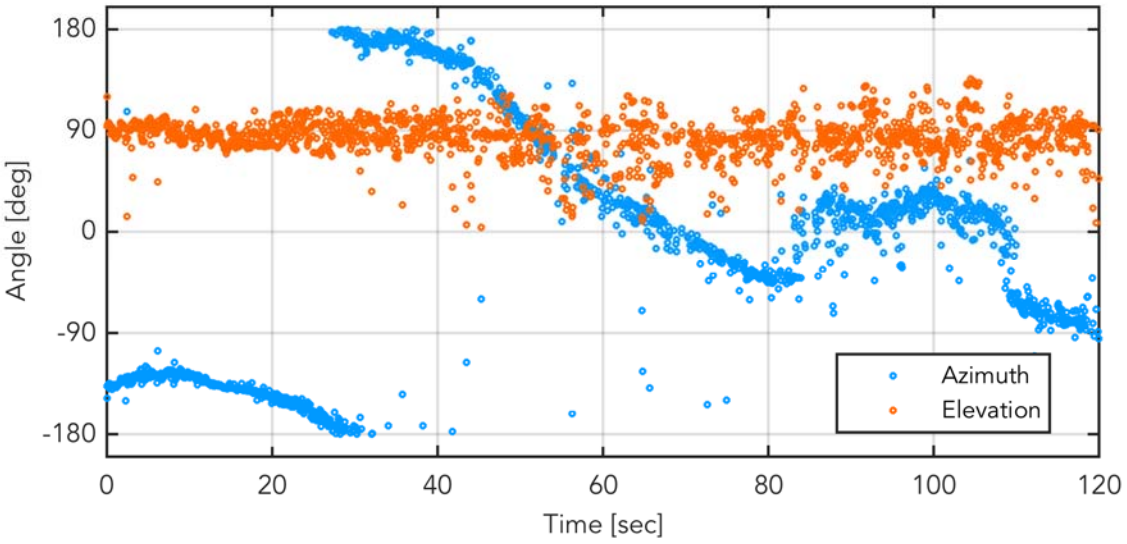

Figure 18: Bearing of R.V. Robertson over a 2 minute period on 6/18/2014.

The primary source of sound was the Robertson's engines. As can be seen in Figure 18, estimates of source elevation remain around 90 degrees. The Raft proceeded to rotate over the 2 minute period, which is visible in the azimuth angle of incoming sound from the Robertson.

Because only two hydrophones were intact during the deployment on 8/25 on the Kviachak River, the resolution of the source localization calculation is significantly less fine (Figure 19). Furthermore, it was only possible to estimate the elevation of incoming plane waves from the vertically oriented hydrophone pair.

Because the horizontal displacement between the RivRaft and RivGen is much greater than their vertical displacement, elevation angles near 90 degrees are not surprising. However, the variation in angle with longshore position, and particularly the abrupt change in angle from -20 m to -10 m, are peculiar.

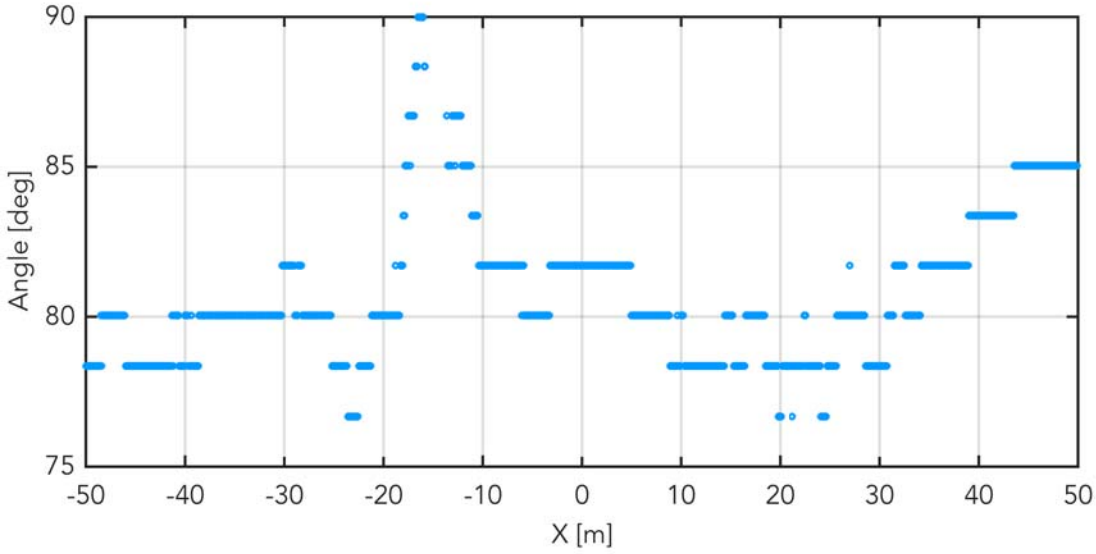

Figure 19: Elevation of incoming plane waves, Optimal 1.

Chapter 4. DISCUSSION

4.1 Sound Characteristics and Potential Sources

The tones centered around 100, 200, and 300 Hz (H1, H2, and H3, Figure 13), appear only during turbine operation, with magnitude and frequency correlated with the turbine rotation rate (Figure 16). More information would be required to definitively identify the source of the sounds, but the hypothesis that the sounds are related to generator operation is consistent with both their harmonic structure and the expected fundamental frequency of vibration of the generator (personal communication, Ocean Renewable Power Company).

Another possible explanation is turbine blade vibration. Effort has been made to model blade vibration in hydrokinetic turbines, though this work has focused mostly on horizontal axis turbines, and not cross flow designs [9]. Tones from blade vibration would be expected to occur at particular modes and would not be expected to vary with rotation rate. Furthermore, RivGen's blades are not cantilevered, as in a horizontal axis turbine, but supported at both ends and at intermediate points along their length, resulting in a higher overall stiffness that would be less likely to vibrate at the observed frequencies. Consequently, while blade vibration due to turbulence is likely to contribute to both optimal and braked levels, blade vibration is unlikely to be the source of the observed tones.

In addition to the distinct tones, a broadband "clicking" sound is noted and audible (Figure 12). This sound occurs once per rotation of the turbine. Most of the acoustic energy in these "clicks" is spread across higher frequencies, from 1 to 10 kHz. The source of this sound is unknown, but might be associated with a misaligned bearing and, therefore, not a typical feature of turbine operation.

4.2 Sound Propagation

The water depth at the location of RivGen is approximately 5 m. At this depth, a 100 Hz tone is not expected to excite a proper normal mode, but the higher frequency tones

at 200 and 300 Hz are not below the modal cutoff and thus would be expected to propagate over longer distances, albeit with lower initial intensity. Higher frequencies, such as those associated with the broadband "clicking" sound, may continue to travel with minimal attenuation (indeed, the "clicking" sound was still audible in water depth less than 0.5 m at a distance of over 150 meters from the turbine). Variation in river depth in the along-channel direction may cause similar losses, thus localizing lower frequency sounds in both along- and across-channel directions. Though this may limit the region ensonified by low frequency sound, the nearfield of a 100 Hz tone (O 30 m) is on the same order as the river width (O 150 m).

4.3 Detection of Turbine Sound by Fishes

While it is beyond the scope of this paper to consider the behavioral effects that turbine sound might have on fishes, as this remains an active area of research in the biological research community, there are characteristics of turbine sound and river bathymetry that may be of interest were one to attempt a study of behavioral changes of Kviachak River fishes.

It is not clear whether the observed tones would be detectable by fishes at the ranges that measurements were undertaken. The level of the 1/3 octave band containing the H1 tone (100 Hz) decays to near ambient conditions within 100 m downstream of the source (Figure 17), which provides rough boundaries to the ensonified region. Additionally, the low frequency tones seen in the pressure spectra were not clearly distinguishable in the vertical particle acceleration spectra. The vertical particle acceleration associated with the tones may be masked by the higher accelerations near the water surface. Additionally, the three-dimensional particle acceleration vector was not measured and may be greater in magnitude. Though a suitable audiogram for sockeye salmon (Oncorhynchus nerka) is unavailable, the observed tones are within the approximate hearing range of Atlantic salmon at [2].

Aside from the low frequency tones, particle acceleration associated with other sources of turbine sound is not likely to be detectable by sockeye salmon at similar ranges (e.g., the broadband "clicking" is above the upper hearing limit for these fish). Notably, the acoustic pressure levels associated with recreational fishing traffic occurs at similar frequencies to turbine operation, so a thorough accounting of contextual sources of sound during the fish migration up and down river would be required as part of a behavioral study.

4.4 PERFORMANCE OF 'RIVRAFT' SYSTEM

Deployment and recovery of the RivRaft were difficult because of the raft's size and weight. At least three operators were required to deploy the raft safely and efficiently, and a team of four was preferable. High drag made towing the raft upstream after each drift nearly impossible, and it was found to be easier to ferry the raft atop the skiff between deployments.

The shape of the "chandelier" increased the risk of entanglement with objects in the current, and indeed three hydrophones were damaged while attempting to deploy the raft. Because of the damage to hydrophones, it was not possible to measure the pressure gradient in three dimensions as originally intended. Instead, a 2-hydrophone array was deployed to measure the pressure gradient in the vertical direction.

Vibration of the chandelier spar and the taut lines supporting it may have contributed to recorded low frequency noise (below 10 Hz). Doppler shift caused by the movement of the RivRaft was assessed and found to contribute on the deci-Hertz scale (i.e., negligible effect), and would be expected for any drifting system, but is not significant.

For future measurements of particle motion using coherent, spatially distributed hydrophones, a lighter and more compact design is recommended. A spar buoy (e.g., SWIFT drifter [18]) could be deployed by an individual from the bow of a skiff, and it would not be unreasonable to outfit a similar design with an accelerometer based sensor or hydrophone array with a smaller hydrophone separation.

Chapter 5. CONCLUSIONS

Sound with strong tonal peaks and a harmonic structure at frequencies less that 500 Hz was measured near an operating river hydrokinetic turbine. The frequency and level of the fundamental tone (approximately 100 Hz) were found to vary with the rotation rate of the turbine, suggesting that generator "cogging" is the source of the tones. The level of the fundamental was also found to decay to near ambient levels within 100 m of the turbine (downstream direction). A broadband clicking sound was also measured and seen to occur approximately once per turbine rotation.

Sounds originating from the turbine were shown to be within the frequency range to which sockeye salmon (*Oncorhynchus nerka*) are most sensitive. However, it was not possible clearly distinguish acoustic particle acceleration from background noise at the measurement depth. To do so, it may be necessary to measure at greater depths, where neither particle motion nor pressure take on extreme values. Because salmon are primarily sensors of particle motion, not pressure, it is unclear if they would be capable of detecting turbine sound based on measurement of turbine sound in the form of pressure alone.

Source bearing estimations were conducted using the same array used for particle motion estimation. Though the 4-element array performed well in trials, damage was incurred to hydrophones during deployment on the Kviachak River, leaving only two hydrophones for bearing estimation. Because measurements conducted on the Kviachak River were lower in resolution (owing to the single pair of hydrophones), source bearing estimation was inconclusive.

Finally, the drifting RivRaft platform was stable and seemed to minimize the relative fluid velocity over it hydrophone array. As a result, flow noise was not detectable at frequencies higher than 30 Hz. In spite of this success, the difficult deployment and recovery of the RivRaft severely limited measurement opportunities. Smaller and lighter systems are advised for future measurements of acoustic particle motion.

BIBLIOGRAPHY

[1] D. T. Blackstock, Fundamentals of Physical Acoustics, John Wiley & Sons, Inc, 2000.

[2] A. N. Popper and R. R. Fay, "Rethinking sound detection by fishes," *Hearing Research,* vol. 273, pp. 25-36, 2009.

[3] A. D. Hawkins, A. N. Popper, R. R. Fay, D. A. Mann, S. Bartol, T. J. Carlson, S. Coombs, W. T. Ellison, R. L. Gentry, M. B. Halvorsen, S. Lokkeborg, P. H. Rogers, B. L. Southall, D. G. Zeddies and W. N. Tavolga, "Sound Exposure Guidelines for Fishes and Sea Turtles: A Technical Report," Springer and ASA Press, Cham, Switzerland, 2014.

[4] G. V. Frisk, Ocean and Seabed Acoustics: A Theory of Wave Propagation, Prentice-Hall Inc., 1994.

[5] D. Tonolla, V. Acuna, M. S. Lorang, K. Heutschi and K. Tockner, "A field-based investigation to examine underwater soundscapes of five common river habitats," *Hydrological Processess,* vol. 24, pp. 3146-3156, 29 May 2010.

[6] H. Hubbard and K. Shepherd, "Aeroacoustics of large wind turbines," *J. Acoust. Soc. Am.,* vol. 89, p. 2495, 1991.

[7] G. H. Jang and D. K. Lieu, "The effect of magnet geometry on electric motor vibration," *IEEE Transactions on Magnetics,* vol. 27, no. 6, pp. 5202-5204, November 1991.

[8] M. J. Lighthill, "On sound generated aerodynamically II. Turbulence as a source of sound," *Proceedings of the Royal Society of London. Series A, Mathematical and Physical Sciences,* 23 February 1954.

[9] M. Jonson, J. Fahnline, E. Johnson, M. Barone and A. Fontaine, "Influence of blade solidty on marine hydrokinetic turbines," in *Internoise 2012/ASME NCAD Meeting*, New York City, 2012.

[10] M. Wahlberg, B. Mohl and P. T. Madsen, "Estimating source position accuracy for a large-aperture hydrophone array for bioacoustics," *J. Acoust. Soc. Am.,* vol. Vol 109, no. No. 1, January 2001.

[11] K. V. Mackenzie, "Nine-term equation for sound speed in the oceans," *J. Acoust. Soc. Am.,* vol. 70, no. 3, September 1981.

[12] D. R. Dall'Osto, P. H. Dahl and J. W. Choi, "Properties of the acoustic intensity vector field in a shallow water waveguide," *J. Acoust. Soc. Am.,* vol. Vol 131, no. No. 3, 2012.

[13] F. J. Fahy, Sound Intensity, Elsevier Science Publishers LTD, 1989.

[14] C. Bassett, J. Thomson, P. H. Dahl and B. Polagye, "Flow-noise and turbulence in two tidal channels," *j. Acoust. Soc. Am.,* vol. 135, no. No. 4, p. 1764, April 2014.

[15] B. Wilson, "Rethinking Underwater Sound-Recording Methods to Work at Tidal-Stream and Wave-Energy Sites," in *Marine Renewable Energy Technology and Environmental Interactions*, Dordrecht, Springer Netherlands, 2014, pp. 111-126.

[16] T. Burton, D. Sharpe, N. Jenkins and E. Bossanyi, Wind Energy Handbook, 2nd ed., Wiley, 2011.

[17] D. Forbush, B. Polagye, J. Thomson, B. Fabien, J. Donegan and J. McEntree, "Characterization and control of cross-flow turbine in shear flow," in *3rd Marine Energy Technology Symposium*, Washington D.C., 2015.

[18] J. Thomson, "Wave Breaking Dissipation Observed with "SWIFT" Drifters," *Journal of Atmospheric and Oceanic Technology,* vol. 29, May 2012.